Journal of Alloys and Compounds 509 (2011) 1994-2000
http://dx.doi.org/10.1016/j.jallcom.2010.10.113

Magnetic and structural characterization of Mo-Hitperm alloys with different Fe/Co ratio

C.F. Conde[a], J.M. Borrego[a], J.S. Blázquez[a], A. Conde[a], P. Švec[b] and D. Janičkovič[b]

[a] Departamento de Física de la Materia Condensada. ICMSE-CSIC. Universidad de Sevilla. P.O. Box 1065. 41080 Sevilla, Spain

[b] Department of Metal Physics, Institute of Physics, Slovak Academy of Sciences, Dúbravská cesta 9, 845 11 Bratislava, Slovakia

Abstract

The influence of the Co content on the microstructure and magnetic behavior of a series of amorphous and nanocrystalline $(FeCo)_{79}Mo_8Cu_1B_{12}$ alloys is reported. Changes in the magnetic properties provoked by the microstructural evolution upon different thermal treatments of as-cast samples are analyzed as well. Kinetics of nanocrystallization process can be described by an isokinetic approach. As the Co content in the alloy increases the Curie temperature of the amorphous as-cast samples increases while the crystallization onset temperature decreases. The crystalline volume fraction as well as the mean grain size of the nanocrystals at the end of the nanocrystallization process is slightly higher for the lowest Co content alloy but smaller than in similar Hitperm Mo-free alloys. The average magnetic field and the average isomer shift of the as-cast samples show a linear increase with two slopes with the Co content of the alloy. The same tendency is found for the saturation magnetization. Combined TEM, XRD, and MS data indicate the presence of Mo atoms in the nanocrystals. At the end of the nanocrystallization process the softest magnetic behavior corresponds to the lowest Co content alloy. The second crystallization process provokes a magnetic hardening of these alloys.

Keywords: Nanocrystalline microstructure; Soft magnets; HITPERM alloys; Mo containing alloys.

1. Introduction

Nanocrystalline alloys obtained by primary crystallization of melt-spun amorphous Fe-based precursors have been greatly studied in the last years as they exhibit an exceptional soft magnetic behaviour (high saturation magnetization, high permeability and low core losses), which makes possible their application in magnetic devices [1]. The distinctive two-phase microstructure displayed by these alloys, in which ferromagnetic nanosized Fe-rich crystals are embedded in a ferromagnetic residual amorphous matrix with a lower Curie temperature, is responsible for their remarkable soft magnetic properties, the relevant parameters being the crystalline volume fraction, the size of the nanocrystals and the composition of both the nanocrystalline and the residual amorphous phases. Magnetic interactions among the nanograins throughout the matrix govern the resulting macroscopic properties and, consequently, the Curie temperature of the residual amorphous phase is a decisive parameter in the temperature dependence of the magnetic behaviour of the alloy.

Journal of Alloys and Compounds 509 (2011) 1994-2000
http://dx.doi.org/10.1016/j.jallcom.2010.10.113

Partial substitution of Co by Fe in FeMB (M=Zr,Nb,Hf) was proposed to extend the soft magnetic behaviour of nanocrystalline alloys up to higher temperatures. An important role is played by the early transition metals which have a very low solubility in the alpha-Fe phase and, consequently, will mainly remain in the amorphous matrix. Moreover, due to their small diffusivity in the amorphous phase, they accumulate at the crystal–matrix interface and constrain the growth of the crystalline phase to the nanocrystalline scale. Many studies on Hitperm FeCoZrB and FeCoNbB alloys have been reported [1, 2, 3, 4, 5] but, more recently, FeCoMoB alloys have been paid increasing attention [6]. Mo addition to Fe alloys delays the iron oxidation in this system and affects the thermal stability and magnetic properties of these amorphous alloys, with a significant lowering of the Curie temperature [7, 8, 9, 10, 11, 12].

The work described here focuses principally on a detailed study of the effect of the substitution of Fe by Co on the kinetic, microstructure, hyperfine parameters and magnetic behaviour of the nanocrystallization process in the $(Fe_xCo_1)_{79}Mo_8Cu_1B_{12}$ system.

2. Experimental

Fe-based amorphous ribbons 6 mm wide and about 20 μm thick, of nominal composition $(Fe_xCo_1)_{79}Mo_8Cu_1B_{12}$ with x=12,9,6,4,3,2,1 (Table 1) were synthesized by planar flow casting in air from ingots of the appropriate composition previously prepared by arc melting of high-purity elements in an argon atmosphere. Chemical composition of the ribbons was checked by emission spectrometry with inductively coupled plasma to confirm no detectable deviation of chemical composition.

To characterize the thermal behaviour of the alloys differential scanning calorimetry (DSC) was performed in a Perkin-Elmer DSC-7 and thermomagnetic gravimetry (TMG) in a Perkin-Elmer TGA-7 applying the magnetic field of a small magnet (~20 mT). Changes in the magnetic force acting upon the sample, related to the variations in magnetization with temperature, are recorded as apparent weight changes of the sample.

Microstructure of as-quenched and nanocrystalline samples was analyzed at room temperature by X-ray diffraction (XRD) in a Bruker D8 using Cu-Kα radiation, transmission electron microscopy (TEM) and electron diffraction (ED) in a Philips CM200 operated at 200 kV and Mössbauer spectroscopy (MS) in a transmission geometry using a ^{57}Co(Rh) source. The incident γ-beam was perpendicular to the ribbon plane. Values of the hyperfine parameters were obtained by fitting with NORMOS program [13]. The isomer shift, δ, was quoted relative to the Mössbauer spectrum of an α-Fe foil at room temperature. Magnetic properties were measured at room temperature by vibrating sample magnetometry (VSM) in a Lakeshore 7407.

Pieces of the as-cast ribbons about 2 cm long (for XRD and MS experiments) and 3 mm diameter disks (for TEM and VSM experiments) were heated in vacuum using a halogen-lamp furnace, at a constant heating rate of 10 K/min from room temperature up to selected temperatures chosen to prepare samples with different microstructures corresponding to different stages of the transformation process.

As-quenched and thermally treated disks samples for TEM were polished by Ar ion beam milling in a Gatan PIPS.

3. Results and discussion

3.1 Devitrification process

Devitrification process of the as-cast $(Fe_xCo_1)_{79}Mo_8Cu_1B_{12}$ alloys takes place in two main stages, in the temperature range available for the DSC, with an onset temperature around 700 K. The originally amorphous alloys became nanocrystalline during the first crystallization stage,

Journal of Alloys and Compounds 509 (2011) 1994-2000
http://dx.doi.org/10.1016/j.jallcom.2010.10.113
and the nanocrystals are surrounded by a residual amorphous matrix. The onset and peak temperatures of this first transformation decrease as the Co content increases in the alloy, as previously observed in Finemet [14] and other Hitperm [15] alloys. Figure 1a shows an almost linear dependence of the temperature peak of the first exotherm with the Co content of the alloy. During the second crystallization stage, the alloys became fully crystallized with the formation of some boride phases, and they loose their soft magnetic character. The second stage starts at lower temperatures as the Co content in the alloys increases. Therefore, the thermal stability of the amorphous alloys as well as that of the nanocrystalline two-phase systems are reduced as the Co content in the alloy increases, as previously reported [16,17]. However, compared with similar Co-free alloys the presence of Co decreases the thermal stability of the amorphous alloys but increases that of the nanocrystalline ones [7-11].

Temperature dependence of the low field magnetization, M, of 3 mm diameter disk samples was measured by TMG scans. The thermomagnetic behaviour is similar for all the studied alloys: a first fall to zero in magnetization at the Curie temperature, Tc, of the ferro-paramagnetic transition of the amorphous phase is recorded. Tc increases with the Co content of the alloy (see Fig. 1a) and a linear dependence with two slopes can be established between them. The Tc of the as-cast amorphous phase in these alloys is significantly lower than the observed for similar Hitperm [3] or Finemet [18] Mo-free alloys, as expected from the known effect of Mo addition on the Curie temperature of the alloy [8]. In fact the $Fe_{79}Mo_8Cu_1B_{12}$ alloy is paramagnetic at room temperature [11].

At the crystallization onset temperature an increase in magnetization starts due to the formation of a ferromagnetic α-FeCo(Mo) type phase with higher Tc. Therefore, as the Co content of the alloy increases, the Curie temperature of amorphous phase is significantly shifted to higher temperatures while the crystallization onset temperature decreases, which provoke that the decrease in magnetization at the Curie transition and its increase at the crystallization onset can overlap in temperature, as occurs for the higher Co content studied alloys [16].

At about 1000 K, temperatures that coincide with those of the second DSC exotherm, a drastic decrease in M is observed although zero magnetization is not reached. Finally, at higher temperature, the new fall in M is associated to the Curie transition of the α-FeCo(Mo) phase (which Tc around 1100K increases with the Co content). TMG plots of fully crystalline samples show the existence of, at least, two magnetic phases.

3.2. Crystallization kinetics

Kinetics characterization of the nanocrystallization process included both non isothermal and isothermal data. Non-isothermal nanocrystallization kinetics was studied from calorimetric data using different kinetic models. The Kissinger method (for samples heated at 2.5, 5, 10, 20, 40 and 80 K/min) allows to obtain a mean value for the apparent activation energy, which decreases from 3.6 to 2.7 eV as the Co content of the alloy increases as shown in Fig. 1b. These values are similar to those found for other Hitperm alloys with Nb [19] and Mn [20] and Nanoperm with Mo [10], or Zr [1] alloys.

A non-isothermal method to obtain local values of Avrami exponent, n, as a function of the crystalline fraction, X, from a single DSC scan and an estimation of the activation energy of the process under the approach of isokinetic transformations [21] has been used. As for the Co free alloy [11] the isokinetic condition is fulfilled for all the studied alloys, as values of the local Avrami index n(X) derived from this approach for DSC data obtained at different heating rates are coincident. Figure 2a shows n(X) values obtained for the x=12 alloy heated at different heating rates. Figure 2b shows n(X) plots obtained for all the studied alloys heated at 10 K/min. Low values of n(X) are obtained as usually found for nanocrystallization processes. Other non-isothermal approaches are in very good agreement with the isokinetic results: Gao-Wang method [22] also supplies a value of n~1, calculated at the peak temperature of the

Journal of Alloys and Compounds 509 (2011) 1994-2000
http://dx.doi.org/10.1016/j.jallcom.2010.10.113
nanocrystallization process (X~0.2), which agrees with the n value obtained for low crystalline volume fractions from the isokinetic approach and is similar to that usually found for FINEMET alloys. These data are generally described by a soft impingement model [23] and recently by the instantaneous growth approximation model [24].

The isothermal kinetics was studied from TMG data for the lower content alloys. Taking into account the magnetic character of the nanocrystalline phase formed, the evolution of the crystallized fraction with time, X(t), can be estimated from the relative change of the magnetization of the sample with the time [25]. Analysing the X(t) dependence in the frame of Johnson-Mehl-Avrami-Kolmogorov (JMAK) theory [26] the plot of ln[-ln(1-X)] vs. ln[t-t_0], where t_0 is the induction time, should be a straight line with the Avrami index, n, as slope. A local Avrami exponent, n(X), can be obtained from the derivative of ln[-ln(1-X)] with respect to ln[t-t_0]. The corresponding curve is shown in Figure 2c (shorter line) for the isothermal transformation of x=12 alloy taken at 688 K. The evolution is similar to that found for different annealing temperatures of the studied alloys. For a better comparison Figure 2c also shows the n(X) values obtained for x=12 alloy through the isokinetic approach for a heating rate of 10 K/min. The value of the local Avrami exponent obtained by the Johnson–Mehl–Avrami plot is in good agreement with that calculated from the isokinetic approach as shown in these plots. Therefore, a good agreement is found between isothermal and non isothermal results describing a low value of the local Avrami exponent (~1) which decreases as the crystalline fraction increases and remains almost constant at high values of X. The first part of the transformation would be mainly due to nucleation (0-1) and the second part would correspond to a progressive saturation of the nucleation sites and to a strongly inhibited crystal growth.

3.3 Microstructure

Room temperature X-ray diffraction patterns of the as-cast samples show their amorphous character. For samples pre-heated up to temperatures inside the first DSC exotherm, X-ray scans only show the characteristic lines of the α-FeCo(Mo) type phase along with a broad maximum revealing the residual amorphous phase. The presence of Mo atoms in the crystals can also be considered [6, 12]. As the Co content of the alloy increases the lattice parameter of the α-FeCo(Mo) phase decreases (see Figure 3) in a similar way of the corresponding binary FeCo alloy [27]. This is an indication of a larger Co content in the crystals as the Co content increases in the alloy.

X-ray patterns of samples heated up to the end of the second DSC exotherm show that they are fully crystallized, and besides the α-FeCo(Mo) phase some boride-type phases mainly $(FeCo)_{23}B_6$-type are identified.

Crystalline volume fraction in the nanocrystalline two-phase system was estimated from a deconvolution of the main X-ray intensity peak to separate the (1 1 0) line of the α-FeCo(Mo) crystals and the amorphous halo intensities. Because of the high metalloid content of the residual amorphous matrix against the metal-rich crystals, the different mean scattering power of the two phases was taken into account in the calculation of the crystalline volume fraction. The crystalline volume fraction at the end of the primary crystallization is strongly affected by the presence of Co in the alloy, decreasing from about 68 % for the Co free alloy to 57-55 % for the Co containing alloys, showing a slight decrease for the higher Co content studied alloy in agreement with the above described enthalpy data, and with previous results on Nb containing HITPERM alloys [3,28].

Mean grain size (~5 nm) of the α-FeCo(Mo) nanocrystals, estimated from Scherrer's formula from full width at half maximum of (110) crystalline reflection peak, is not significantly affected during the nanocrystallization process and is nearly independent of the Co content in the alloy, with differences inside the experimental error, only a very slight decrease

Journal of Alloys and Compounds 509 (2011) 1994-2000
http://dx.doi.org/10.1016/j.jallcom.2010.10.113
as the Co content increases should be noted. Values of the mean grain size and the crystalline volume fraction at the end of the nanocrystallization process for these Mo containing alloys are lower than those found for analogous FeCoNbCuB alloys [3].

TEM bright field images in Figure 4 left show a closer view of the microstructure of samples of different alloys heated up to the end of their first DSC event. The crystals of α-FeCo(Mo) phase mainly appear as single grains homogeneously distributed in a residual amorphous matrix, although aggregates of a few of the smallest grains can also be observed which increase in number as the Co content increases in the alloy. The grain size distribution (Fig. 4 right) becomes narrower, and shows a slight decrease in the mean grain size as the Co content in the alloy increases in agreement with previous XRD observation. For all the compositions the mean grain size is smaller when measured in TEM micrographs than from X-ray patterns as the aggregation of grains can be detected from TEM.

3.4 Soft magnetic properties

Figure 5 shows the Mössbauer spectra of as-quenched samples taken at 300 K. The six-line pattern characteristic of amorphous ferromagnetic alloys progressively collapses as the Co content of the alloy decreases, as the Curie temperature approaches to room temperature. The data were fitted using a discrete hyperfine magnetic field distribution (HFD) with the quadrupolar splitting averaged to zero. In order to reproduce the asymmetrical shape of the spectra, a linear correlation between the hyperfine magnetic field and the isomer shift of the components of the distribution was introduced.

The hyperfine magnetic field distributions corresponding to Mössbauer spectra are shown in Fig. 5 (right). Values of B_{hf} below 5 T could be ascribed to Fe atoms in paramagnetic sites, as the fitting method used cannot distinguish between low hyperfine values and paramagnetic contributions. Their bimodal behaviour in HFD reveals the presence of two main kinds of iron environments in the amorphous as-cast state and HFDs can be approximately described by means of two Gaussian components. The high field component (HF) can be ascribed to sites where Fe atoms are preferentially surrounded by Fe, Co and B atoms and the low field (LF) one to Fe atoms preferentially surrounded by Mo and B atoms [29]. Figure 6a shows the increase of the Gaussian maxima as the Co content increases.

Figure 6b shows the increase of the average hyperfine magnetic field, $<B_{hf}>$, with the Co content which can be fitted by a two linear steps of slopes: 0.87(3) T for at. % Co atom for a Co content up to 16 at. % and 0.14 (1) T at. % Co for a Co content up to 40 at. %, in agreement with the tendency observed for Tc.

Figure 6c shows the dependence of the average isomer shift, as a function of the Co content of the alloy. A linear increase of $<\delta>$ with at. % Co with two slopes is also found.

Figure 7 shows the Mössbauer spectra of partially crystallized samples of the different studied compositions, after heated up to the end of their first DSC event, taken at 300 K. The experimental data were fitted using a discrete set of sextets (A, B, C and D for samples with x=1-4 and 6; and A, B, C' for samples with x=9 and 12) and two hyperfine field distributions (from 0 to 20 T, D_1 and from 15 to 32 T, D_2) which can be roughly ascribed to Fe atoms in the amorphous and Fe atoms in the interface, respectively. As Co content increases the distinction between these two environments becomes troublesome.

Due to the complexity in fitting values of the hyperfine magnetic field and the isomer shift of the crystalline sextets (Table 2) were fixed. Table 3 shows the relative contribution of the crystalline sextets for the studied alloys.

The crystalline volume fraction, X, was calculated from the absorption areas of the crystalline sextets plus the interface contribution (D_2) relative to the total area (Figure 8), considering a calculated composition of the FeCoMo nanocrystals by assuming a 2 at. % content of Mo [30] and a nominal content of Co [15, 31]. The result was X ~ 50-55%.

Journal of Alloys and Compounds 509 (2011) 1994-2000
http://dx.doi.org/10.1016/j.jallcom.2010.10.113

Figure 9 shows the average hyperfine magnetic field and average isomer shift of the amorphous phase (D_1), the interface (D_2) and the crystalline sextets (S) of nanocrystalline samples as a function of the Co content.

It can be also clearly observed a different magnetic texture of sample x=1 when the relative intensities of the spectra lines of the different samples are compared. The fitting of the spectra, assuming an identical magnetic texture of both crystalline grains and the residual amorphous matrix, leads to an orientation of $\theta=55^{o}$ of the γ-beam with respect to the ribbon plane for x=1, consistent with a random distribution of magnetic moment directions. For the rest of the samples, a value of $\theta=30^{o}$ indicates an out of plane distribution of magnetic moments.

VSM results indicate that for each composition the relaxation process decreases the saturation magnetization, M_s, of the amorphous samples while the nanocrystallization process increases it. Plots of Figure 10 show the values of M_s against the Co content of the alloy for relaxed samples and for samples pre-heated up to 800 K, temperature that corresponds to the end of the nanocrystallization process. The represented values were measured from hysteresis loops taken at room temperature at the VSM with a maximum applied field of 5KOe.

For relaxed as well as for nanocrystalline samples M_s increases with the Co content of the alloy up to ~15 at. % Co in accordance with the observed dependence of the hyperfine magnetic field (see Fig. 9). For each composition M_s increases with the volume fraction of bcc-FeCo(Mo) nanocrystals during the nanocrystallization process.

The coercive field, H_c (inside the experimental errors of this technique for the range of H_c values ~1 Gauss) measured from the same hysteresis loops shows a similar value for the relaxed amorphous samples while the softest nanocrystalline sample corresponds to the lowest Co content alloy.

4. Conclusions

A study of relationship between structural and magnetic properties of a set of FeCoMoCuB HITPERM-type alloys by a variety of complementary techniques is reported.

The devitrification process of these FeCoMoCuB alloys starts at around 700 K and takes place in two main stages. The alloys, originally amorphous, became nanocrystalline during the first crystallization stage. During the second crystallization stage the alloys became fully crystallized losing their soft magnetic character.

Increasing Co content of the alloy decreases the thermal stability of the amorphous phase and that of the nanocrystalline alloy. Nanocrystallization kinetics results based on isothermal (TMG) and non-isothermal (DSC) experiments agree describing a strongly inhibited grain growth process. The nanocrystalline microstructure is similar for all the alloys. The crystalline volume fraction at the end of the nanocrystallization process is practically not affected with the increase of Co in the alloy, although it is lower than in the corresponding Co free alloy. The lattice parameter of the α-FeCo(Mo) phase nanocrystals decreases as the Co content in the alloy increases in agreement with the increased Co content of the grains. The size of the nanocrystals at the end of the nanocrystallization process slightly decreases as the Co content increases in the alloy.

Mössbauer spectra of amorphous and heat treated samples were analyzed in the frame of three different contributions: pure crystalline, interface and amorphous contribution. Average hyperfine magnetic field of the crystalline contribution is higher for alloys with 15-20 at. % of Co. Comparison between TEM, XRD and Mössbauer data indicates that some Mo could be present inside the nanocrystals.

The magnetic behaviour at room temperature of the as cast, relaxed and nanocrystalline alloys shows a saturation magnetization that increases with the Co content in the alloy. For each studied composition M_s increases with the crystalline volume fraction during the nanocrystallization process.

Journal of Alloys and Compounds 509 (2011) 1994-2000
http://dx.doi.org/10.1016/j.jallcom.2010.10.113

Mo content provokes low values of the Curie temperature of these amorphous alloys, even below room temperature for the Co free alloy. Changing the Fe/Co ratio allows to increase the Curie temperature of the amorphous alloys for these compositions between room temperature and ~ 800 K, and therefore, allows tuning the temperature at which the maximum magnetocaloric effect takes place opening a possibility for these alloys as potential low cost magnetic refrigerants.

Acknowledgements

This work was supported by the Spanish Ministry of Science and Innovation and EU FEDER (Project MAT 2007-65227), the PAI of the Regional Government of Andalucía, VEGA 2/0157/08 and APVV-0413-06.

Journal of Alloys and Compounds 509 (2011) 1994-2000
http://dx.doi.org/10.1016/j.jallcom.2010.10.113
Table 1. Co content (at. %) of the studied alloys.

x	at. % Co
1	39.5
2	26.3
3	19.8
4	15.8
6	11.3
9	7.9
12	6.1

Table 2. Hyperfine magnetic field and isomer shift of the crystalline sextets for the studied alloys.

	A	B	C	C’	D
B_{hf} (T)	33.0	34.5	35.6	36.5	37.0
δ (mm/s)	0.0000	0.0136	0.0286	0.0286	0.0504

Table 3. Relative contribution (%) of the crystalline sextets for the studied alloys.

x	A	B	C	C’	D
1	27.8	43.9	24.4		3.9
2	17.7	27.2	31.8		23.3
3	14.6	21.5	33.8		30.1
4	14.5	22.3	33.7		29.5
6	21.6	32.0	33.0		13.4
9	28.0	57.0		15.0	
12	33.4	57.6		9.0	

Journal of Alloys and Compounds 509 (2011) 1994-2000
http://dx.doi.org/10.1016/j.jallcom.2010.10.113

Figure captions

Figure 1. Curie temperature of the as-cast alloys (T_C) and peak temperatures of the 1 first DSC event (T_P) (a). Apparent activation energies of the nanocrystallization process versus at. % Co content in the alloys (b).

Figure 2. n(X) from DSC scans of x=12 alloy taken at different heating rates (a). n(X) from DSC scans of the studied alloys taken at 10 K/min (b). Comparison between isothermal TMG (shorter line) and non-isothermal DSC (taken at 2.5 K/min) results for the x=12 alloy (c).

Figure 3. Lattice parameter of the α-FeCo(Mo) phase at the end of the 1 first DSC event as a function of the Co content of the alloy. Values of those of FeCo binary alloy are included for comparison.

Figure 4. TEM bright field images obtained for samples of 0 at. % Co and x=12, 6, 3, 1 alloys heated up to the end of their first crystallization event (left) and their corresponding distribution of grain sizes (right).

Figure 5. Mössbauer spectra of as-quenched samples taken at 300 K and their corresponding hyperfine field distributions.

Figure 6. Peak position of high field component (HF) and low field component (LF) of the hyperfine field distributions (a); the average hyperfine magnetic field (b) and the average isomer shift (c), corresponding to as-quenched samples as a function of the Co content.

Figure 7. Mössbauer spectra of partially crystallized samples, after heated up to the end of the first DSC event, taken at 300 K, and their hyperfine field distributions corresponding to the amorphous phase (D1) and the interface (D2).

Figure 8. Area of the amorphous phase (D1), the interface (D2) and the crystalline sextets (S) of nanocrystalline samples as a function of the Co content.

Figure 9. Average hyperfine magnetic field, $\langle B_{hf} \rangle$, and average isomer shift $\langle \delta \rangle$, of the amorphous phase (D1), the interface (D2) and the crystalline sextets (S) of nanocrystalline samples as a function of the Co content of the alloy.

Figure 10. Saturation magnetization, M_s, versus at. % Co content in the alloys for relaxed and nanocrystalline samples.

Journal of Alloys and Compounds 509 (2011) 1994-2000
http://dx.doi.org/10.1016/j.jallcom.2010.10.113

References

[1] M.E. McHenry, M.A. Willard, D.E. Laughlin, Prog. Mater. Sci. 44 (1999) 291.
[2] M. Müller, H. Grahl, N. Mattern, U. Kühn, B. Schnell, J. Magn. Magn. Mater. 160 (1996) 284.
[3] F. Johnson, P. Hughes, R. Gallagher, D.E. Laughlin, M.E. McHenry, M.A. Willard, V. G. Harris, IEEETM 37 (2001) 2261.
[4] C.F. Conde, J.S. Blazquez, A. Conde, in: B. Idzikowski, et al. (Eds.), Properties and Applications of Nanocrystalline Alloys from Amorphous Precursors Vol. 1, Kluwer Academic Publishers, Dordrecht, Holanda; 2005, p. 111.
[5] J.S. Blázquez, V. Franco, C.F. Conde, A. Conde, J. Ferenc, T. Kulik, L.F. Kiss, J. Appl. Phys. 105 (2009) 093928.
[6] M. Paluga, P. Švec, D. Janičkovič, D. Muller, P. Mrafko, M. Miglierini, Rev. Adv. Mater. Sci. 18 (2008) 481.
[7] B. Idzikowski, J. Baszynski, I. Skorvánek, K.-H. Müller, D. Eckert, J. Magn. Magn. Mater. 177-181 (1998) 941.
[8] M. Müller, H. Grahl, N. Mattern, B. Schnell, Mat. Sci. Eng. A 304–306 (2001) 353.
[9] M. Miglierini, I. Toth, M. Seberıni, E. Illekova, B. Idzikowski, J. Phys.: Condens Matter 14 (2002) 1249.
[10] E. Illekova, D. Janičkovič, M. Miglierini, I. Skorvanek, P. Švec, J. Magn. Magn. Mater. 304 (2006) e636.
[11] C.F. Conde, J.S. Blázquez, V. Franco, A. Conde, P. Švec, D. Janičkovič, Acta Mater. 55 (2007) 5675.
[12] M. Miglierini, J. Non-Cryst. Solids 354 (2008) 5093.
[13] R.A. Brand, J. Lauer, D.M. Herlach, J. Phys. F: Met. Phys. 13 (1983) 675.
[14] J.M. Borrego, C.F. Conde, A. Conde, J.M. Greneche, J. Non-Cryst. Solids 287 (2001) 120.
[15] J.S. Blázquez, J.M. Borrego, C.F. Conde, A. Conde, J.M. Greneche, J. Phys.: Condens Matter 15 (2003) 3957.
[16] C.F. Conde, A. Conde, D. Janičkovič, P. Švec, J. Magn. Magn. Mater. 304 (2006) e739.
[17] C.F. Conde, A. Conde, Reviews on Adv. Mat. Sci. 18 (2008) 565.
[18] V. Franco, C.F. Conde, A. Conde, P. Ochin, J. Non-Cryst. Solids 287 (2001) 366.
[19] J.S Blázquez, C.F. Conde, A. Conde, J. Non-Cryst. Solids 287 (2001) 187.
[20] C.F. Conde, A. Conde, P. Švec, P. Ochin, Mat. Sci. Eng. A 375–377 (2004) 718.
[21] J.S. Blázquez, C.F. Conde, A. Conde, Acta Mater. 53 (2005) 2305.
[22] Y.Q. Gao, W. Wang, J. Non-Cryst. Solids 81 (1986) 129.
[23] M.T. Clavaguera-Mora, N. Clavaguera, D. Crespo, T. Pradell, Prog. Mater. Sci. 47 (2002) 559.
]24] J.S. Blázquez, M. Millán, C.F. Conde, A. Conde, Phil. Mag. 87 (2007) 4151.
[25] C.F. Conde, A. Conde, Mat. Lett. 21 (1994) 409.
[26] J.W. Christian, in The Theory of Transformation in Metals and Alloys, Part 1: Pergamon, Oxford; 1975, p. 542.
[27] R.M. Bozorth, in: Ferromagnetism, Van Nostrand, Princeton, NJ, 1968, p. 192.
[28] J.S. Blázquez, V. Franco, C.F. Conde, A. Conde, J. Magn. Magn. Mater. 254–255 (2003) 460.
[29] M. Miglierini, J. Phys.: Condens. Matter 6 (1994) 1431.
[30] A. Fernandez Guillemet, Bull. Alloy Phase Diagrams 3 (1982) 359.
[31] Y. Zhang, J.S. Blázquez, A. Conde, P.J. Warren, A. Cerezo, Mater. Sci. Eng. A 353 (2003) 158.

Journal of Alloys and Compounds 509 (2011) 1994-2000
http://dx.doi.org/10.1016/j.jallcom.2010.10.113

Figure 1

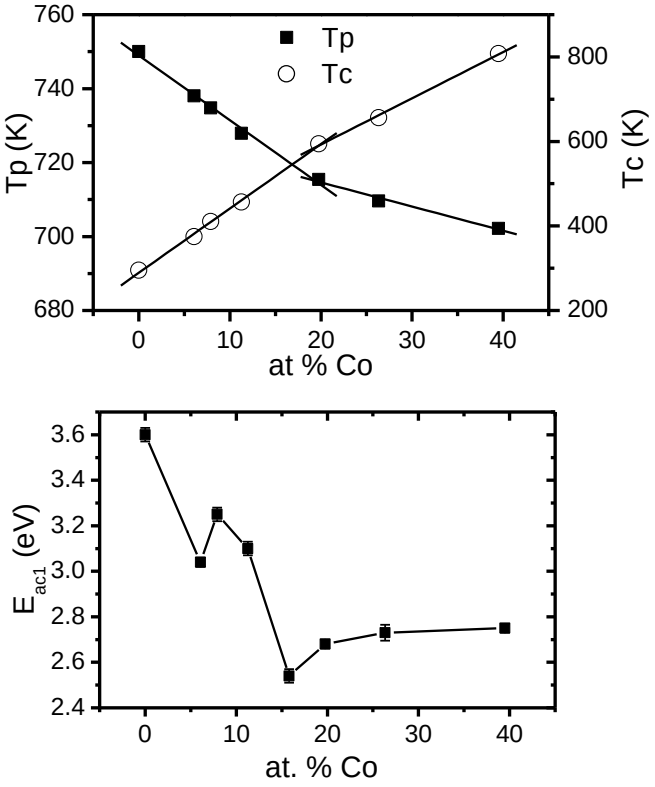

Journal of Alloys and Compounds 509 (2011) 1994-2000
http://dx.doi.org/10.1016/j.jallcom.2010.10.113

Figure 2

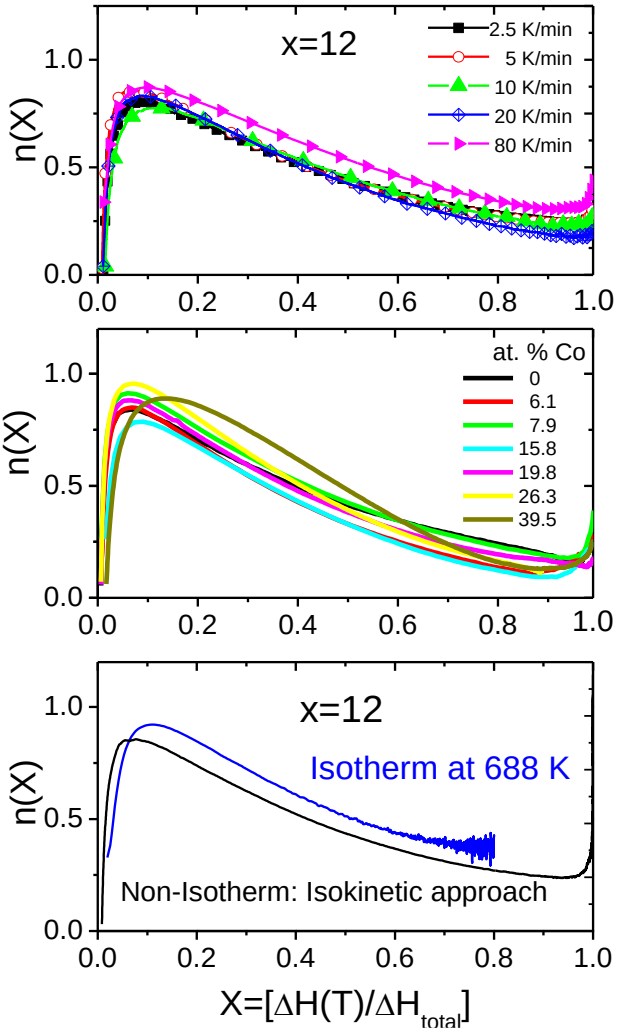

Journal of Alloys and Compounds 509 (2011) 1994-2000
http://dx.doi.org/10.1016/j.jallcom.2010.10.113

Figure 3

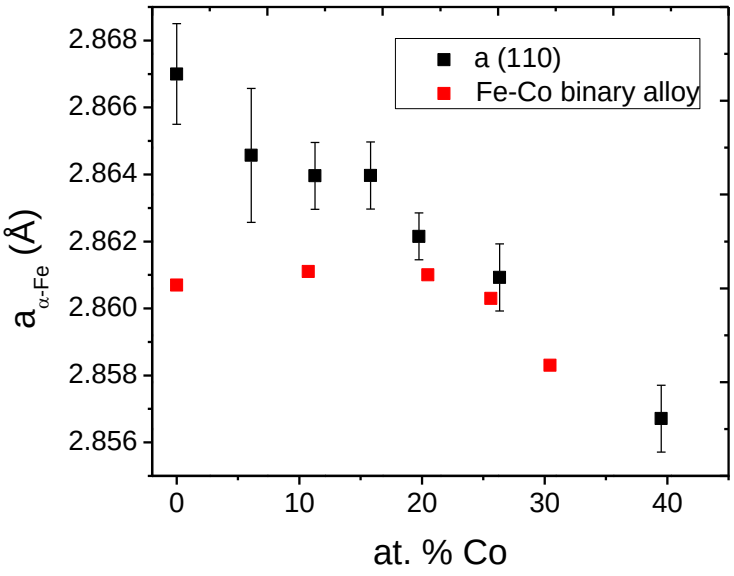

Journal of Alloys and Compounds 509 (2011) 1994-2000
http://dx.doi.org/10.1016/j.jallcom.2010.10.113

Figure 4

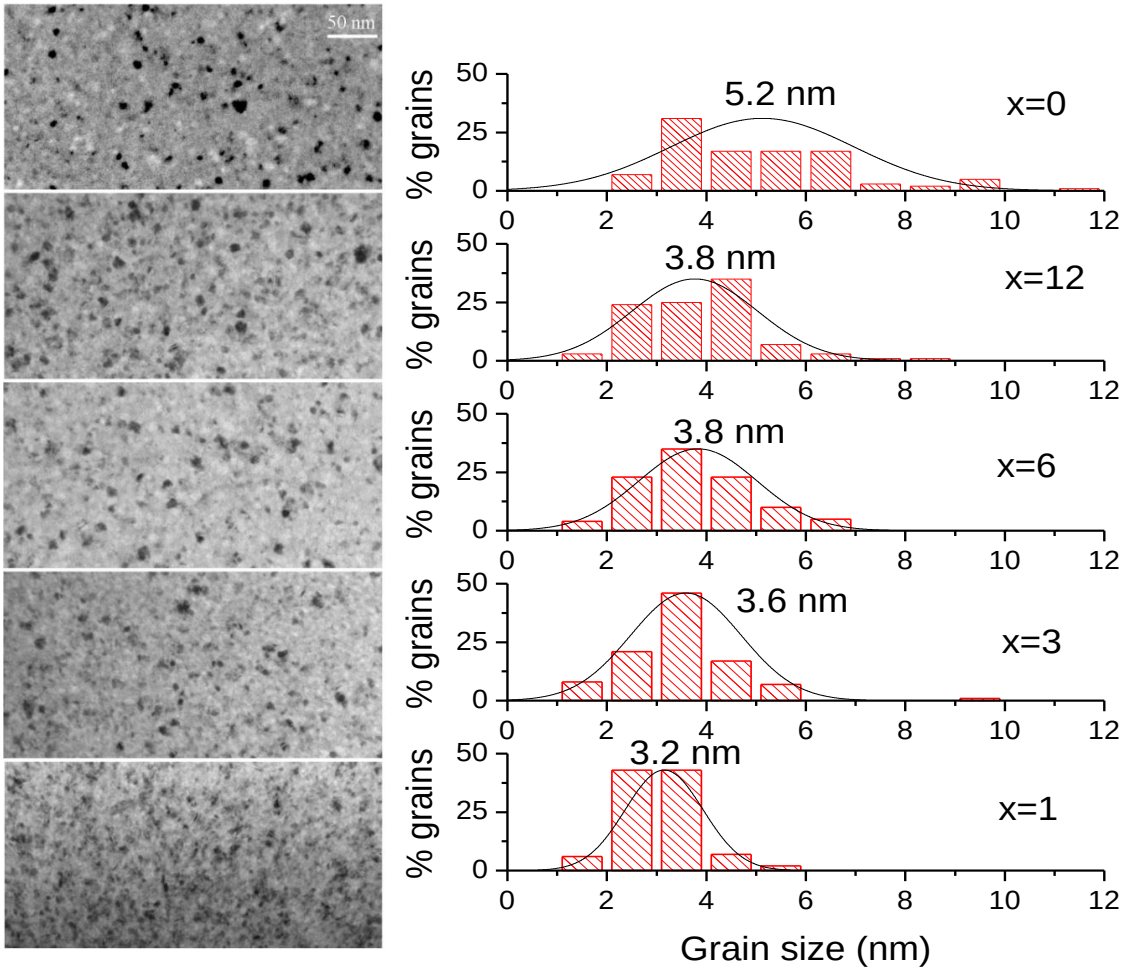

Journal of Alloys and Compounds 509 (2011) 1994-2000
http://dx.doi.org/10.1016/j.jallcom.2010.10.113

Figure 5

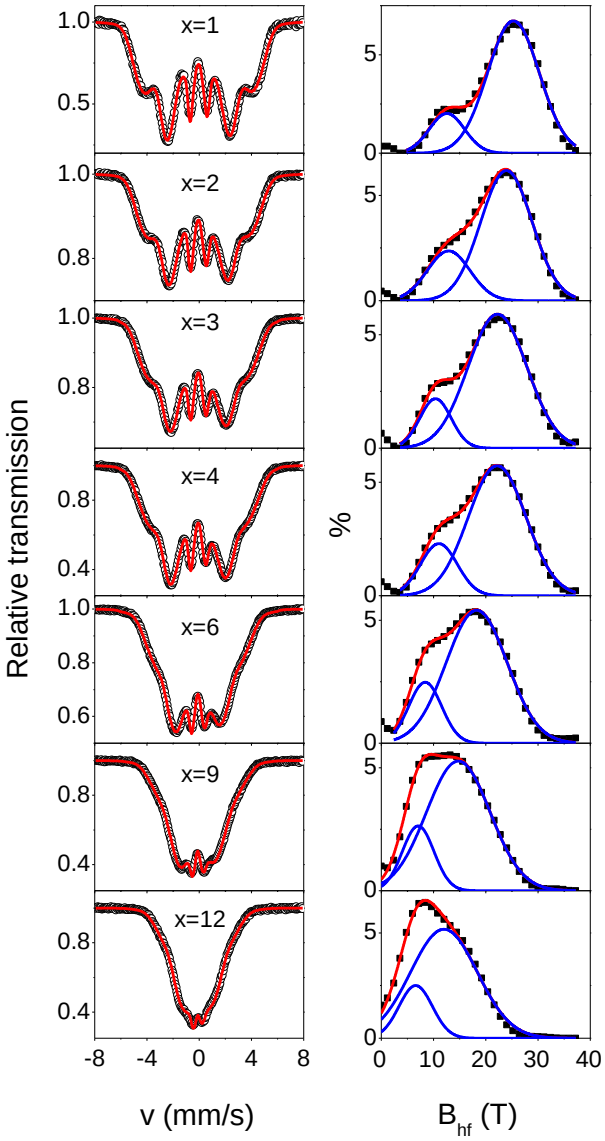

Journal of Alloys and Compounds 509 (2011) 1994-2000
http://dx.doi.org/10.1016/j.jallcom.2010.10.113

Figure 6

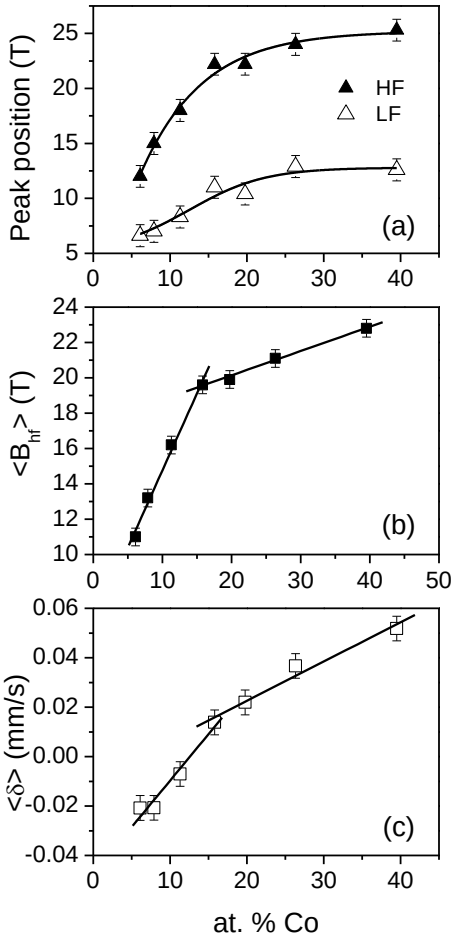

Journal of Alloys and Compounds 509 (2011) 1994-2000
http://dx.doi.org/10.1016/j.jallcom.2010.10.113

Figure 7

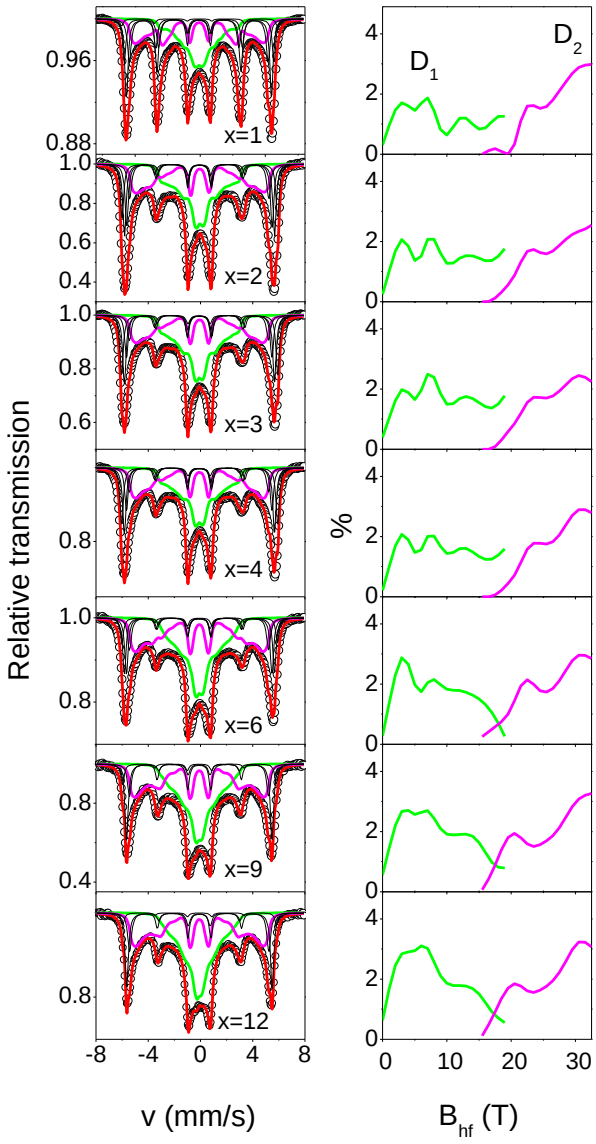

Journal of Alloys and Compounds 509 (2011) 1994-2000
http://dx.doi.org/10.1016/j.jallcom.2010.10.113

Figure 8

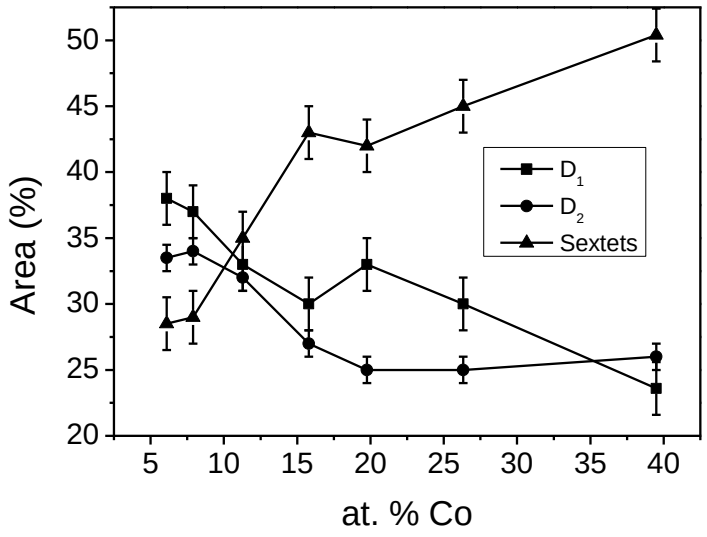

Journal of Alloys and Compounds 509 (2011) 1994-2000
http://dx.doi.org/10.1016/j.jallcom.2010.10.113

Figure 9

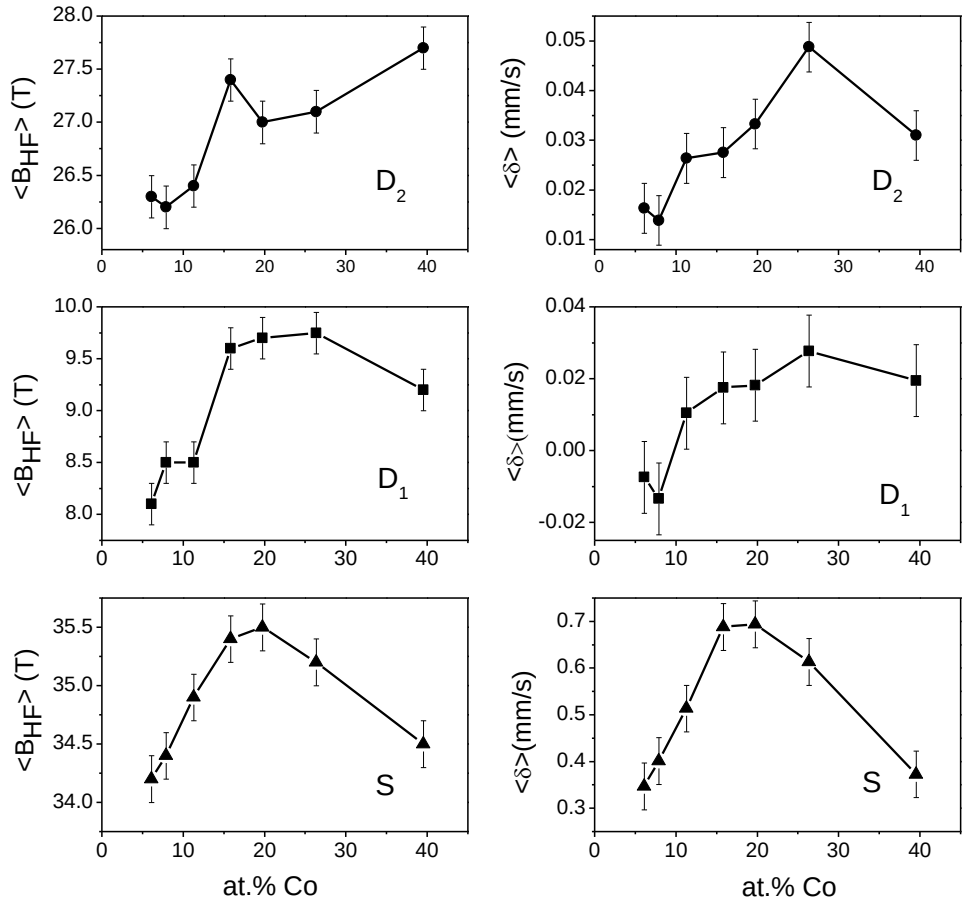

Journal of Alloys and Compounds 509 (2011) 1994-2000
http://dx.doi.org/10.1016/j.jallcom.2010.10.113

Figure 10